

# Dilepton production and $m_T$ -scaling at BEVALAC/SIS energies \*

E. L. Bratkovskaya<sup>1</sup>, W. Cassing<sup>1</sup>, R. Rapp<sup>2</sup> and J. Wambach<sup>3</sup>

<sup>1</sup>Institut für Theoretische Physik, Universität Giessen

D-35392 Giessen, Germany

<sup>2</sup> Department of Physics and Astronomy, State University of New York,

Stony Brook, NY 11794-3800, U.S.A.

<sup>3</sup> Insitut für Kernphysik, TU Darmstadt, Schloßgartenstr. 9,

D-64289 Darmstadt, Germany

## Abstract

We present a dynamical study of  $e^+e^-$  production in C + C and Ca + Ca collisions at BEVALAC/SIS energies on the basis of the covariant transport approach HSD employing momentum-dependent  $\rho$ -meson spectral functions that include the pion modifications in the nuclear medium as well as the polarization of the  $\rho$ -meson due to resonant  $\rho-N$  scattering. We find that the experimental data from the DLS collaboration cannot be described within the  $\rho$ -meson spectral function approach. A dropping  $\eta$ -mass scenario leads to a good reproduction of the DLS dilepton data, however, violates the  $m_T$ -scaling of  $\pi^0$  and  $\eta$  spectra as observed by the TAPS collaboration as well as  $\eta$  photoproduction on nuclei.

PACS: 25.75+r 14.60.-z 14.60.Cd

Keywords: relativistic heavy-ion collisions, leptons

---

\*Work supported by BMBF and GSI Darmstadt.

## I. INTRODUCTION

The mechanism of chiral symmetry restoration at high baryon density is of fundamental importance for the understanding of QCD [1,2], but a clear experimental evidence has not been achieved, so far. In this respect, dileptons are particularly well suited for an investigation of the early phases of high-energy heavy-ion collisions because they can leave the reaction volume essentially undistorted by final-state interactions. Indeed, dileptons from heavy-ion collisions have been measured by the DLS collaboration at the BEVALAC [3–6] and by the CERES [7,8], HELIOS [9,10], NA38 [11] and NA50 [12] collaborations at SPS energies.

Various theoretical calculations [13–17] fail in describing the spectral shape of the dilepton yield for nucleus-nucleus collisions at SPS energies when employing a 'free'  $\rho$ -meson form factor but are successful when using a dropping  $\rho$ -mass in the medium. However, a more conventional approach including the change of the  $\rho$ -meson spectral function in the medium due to the coupling of  $\rho$ ,  $\pi$ ,  $\Delta$  and nucleon dynamics along the lines of Refs. [18–21] was found to be (roughly) compatible with the CERES data [14,21] as well, whereas the dimuon data of the HELIOS-3 collaboration [9] could only be described satisfactorily when including 'dropping' meson masses [22,23] according to Hatsuda and Lee [24]. Meanwhile, our knowledge on the  $\rho$  spectral function has improved since – as first pointed out by Friman and Pirner [25] – resonant  $\rho$ - $N$  interactions in p-wave scattering significantly enhance the strength in the vector-isovector channel at low invariant mass. In fact, the CERES data for S + Au at 200 A GeV and Pb + Au at 160 A GeV, using an expanding fireball model, were found to be compatible within such a hadronic scenario [26]. This general shape of the  $\rho$  spectral function has also been confirmed recently in Ref. [27] where the authors find a significant smearing of the  $\rho$  strength at low  $\rho$  momenta due to a selfconsistent evaluation of the resonance widths. Furthermore, as shown in Refs. [28,29], both scenarios (dropping mass and  $\rho$ -meson broadening) are compatible with QCD sum rules.

The thermodynamical result of Ref. [26] was supported by HSD transport calculations

[30] where an improved  $\rho$  spectral function (*i.e.* by constraints from  $\gamma p$  and  $\gamma A$  data) was involved. The important conclusion in Ref. [30] was that both the 'dropping mass' scenario [14,22,23,31] as well as the hadronic spectral function approach [26] lead to dilepton spectra which are in good agreement with the experimental data for all systems at SPS energies.

In this respect, it is a natural step to investigate within the same framework dilepton production at BEVALAC energies where quite a different temperature and density regime is probed. From a recent publication of the DLS collaboration [6], it turns out that the new measurements of dilepton yields in A + A collisions have increased by about a factor of 6-7 in comparison to the previous data set [3–5] due to an improvement of the DLS detector and the data analysis correcting for dead time losses. However, the first generation of DLS data were reasonably described by several theoretical models [32–35] without incorporating any medium effects. These various models are consistent in the general tendency that the dilepton pairs of invariant mass below 0.4 GeV are primarily produced from hadronic sources, such as the Dalitz decays of  $\pi^0$ ,  $\Delta$  and  $\eta$  and  $pn$  bremsstrahlung, whereas for  $M \geq 0.4$  GeV the dominant contributions stem from the  $\pi^+\pi^-$  annihilation channel and direct decays of vector mesons ( $\rho, \omega$ ). Since this has led to a fair agreement with the old DLS data the aforementioned theoretical models are not able to explain the new DLS data set [6] without incorporating new ingredients such as vector meson selfenergies.

The DLS collaboration pointed out that the inconsistency between the data and theoretical results – incorporating no medium effects – might be due to a strong underestimation of the  $\eta$  contribution in the model calculations. As found in Ref. [6] the shape of the dilepton yield for  $M \leq 0.4$  GeV is quite similar to that of the  $\eta$  component in the BUU model [35]. The main knowledge about  $\eta$  production in heavy-ion collisions at BEVALAC/SIS energies is provided by the TAPS collaboration [36–38]. However, TAPS measures  $\pi^0$  and  $\eta$  mesons in a small rapidity interval near  $y_{cm}$  whereas the DLS spectrometer covers the forward rapidity region. Within a thermal model calculation – using the TAPS mid-rapidity data and assuming an isotropic  $\eta$  angular distribution – the DLS collaboration found that the  $\eta$  yield

in their rapidity window then is in good agreement with the BUU model predictions [35,39]. The dilepton enhancement observed by the DLS Collaboration thus might be due to a strong anisotropy of the  $\eta$  angular distribution in the center-of-mass system.

In this article we address the DLS 'puzzle' by employing in our transport calculation novel theoretical developments, i.e. in-medium  $\rho$  spectral functions as well as hypothetical in-medium modifications of the  $\eta$  mass. To arrive at more stringent conclusions concerning the  $\eta$  contribution we simultaneously analyze the DLS dilepton data [6] together with the new TAPS data [37,38] with respect to  $m_T$  spectra of  $\pi^0$ 's and  $\eta$ 's as well as  $\eta$  photoproduction on nuclei.

Our paper is organized as follows: In Section 2 we briefly describe the transport approach employed as well as the elementary production channels. Section 3 contains a comparison of our calculations for  $\pi^0$  and  $\eta$   $m_T$ -spectra with the TAPS data. In Section 4 we discuss the  $\rho$  spectral functions which will be applied for calculating the dilepton spectra. Section 5 contains a detailed comparison of the calculated dilepton spectra at BEVALAC energies with the DLS data [6]. In Section 6 we investigate the consequences of a dropping  $\eta$ -mass scenario for  $m_T$ -spectra and dilepton production at BEVALAC/SIS energies as well as  $\eta$  photoproduction on nuclei. The  $\eta$  angular anisotropy is investigated in Section 7 while we close with a summary and discussion of open problems in Section 8.

## II. TRANSPORT MODEL INGREDIENTS

In this work we perform the theoretical analysis along the line of the HSD approach [40] which is based on a coupled set of covariant transport equations for the phase-space distributions  $f_h(x, p)$  of hadron  $h$  [40,41], i.e.

$$\begin{aligned} & \left\{ \left( \Pi_\mu - \Pi_\nu \partial_\mu^p U_h^\nu - M_h^* \partial_\mu^p U_h^S \right) \partial_x^\mu + \left( \Pi_\nu \partial_\mu^x U_h^\nu + M_h^* \partial_\mu^x U_h^S \right) \partial_p^\mu \right\} f_h(x, p) \\ &= \sum_{h_2 h_3 h_4 \dots} \int d^2 d^3 d^4 \dots [G^\dagger G]_{12 \rightarrow 34 \dots} \delta_1^4 (\Pi + \Pi_2 - \Pi_3 - \Pi_4 \dots) \\ & \times \left\{ f_{h_3}(x, p_3) f_{h_4}(x, p_4) \bar{f}_h(x, p) \bar{f}_{h_2}(x, p_2) \right\} \end{aligned}$$

$$- f_h(x, p) f_{h_2}(x, p_2) \bar{f}_{h_3}(x, p_3) \bar{f}_{h_4}(x, p_4) \} \dots \quad (1)$$

In Eq. (1)  $U_h^S(x, p)$  and  $U_h^\mu(x, p)$  denote the real part of the scalar and vector hadron self-energies, respectively, while  $[G^+G]_{12 \rightarrow 34 \dots} \delta_\Gamma^4(\Pi + \Pi_2 - \Pi_3 - \Pi_4 \dots)$  is the ‘transition rate’ for the process  $1 + 2 \rightarrow 3 + 4 + \dots$ . In quantum many-body systems this transition rate is partly off-shell – as indicated by the index  $\Gamma$  of the  $\delta$ -function – with width  $\Gamma \approx \tau_{coll}^{-1}$  where  $\tau_{coll}$  is the average collision rate for the colliding hadrons. In our semi-classical transport approach the on-shell limit  $\Gamma \rightarrow 0$  is adopted which is found to describe reasonably well hadronic spectra in a wide dynamical regime. Note that the on-shell limit has been proven explicitly to be a valid approximation for intermediate energy heavy-ion collisions in Ref. [42]. The hadron quasi-particle properties in (1) are defined via the mass-shell constraint [41],  $\delta(\Pi_\mu \Pi^\mu - M_h^{*2})$ , with effective masses and momenta given by

$$\begin{aligned} M_h^*(x, p) &= M_h + U_h^S(x, p) \\ \Pi^\mu(x, p) &= p^\mu - U_h^\mu(x, p) \quad , \end{aligned} \quad (2)$$

while the phase-space factors

$$\bar{f}_h(x, p) = 1 \pm f_h(x, p) \quad (3)$$

account for fermion Pauli-blocking or Bose enhancement, depending on the type of hadron in the final and initial channel. The dots in Eq. (1) indicate further contributions to the collision term with more than two hadrons in the final/initial channels. The transport approach (1) is fully specified by  $U_h^S(x, p)$  and  $U_h^\mu(x, p)$  ( $\mu = 0, 1, 2, 3$ ), which determine the mean-field propagation of the hadrons, and by the transition rates  $G^\dagger G \delta_\Gamma^4(\dots)$  in the collision term that describe the scattering and hadron production/absorption rates. For more details we refer the reader to Ref. [40].

In addition to the direct production of all mesons in Ref. [40] we treat the production of vector mesons ( $\rho, \omega, \phi$ ) and  $\eta$ 's at low energies also perturbatively. The vector mesons as well as  $\eta$  mesons are produced in baryon-baryon and meson-baryon collisions according to

the elementary production cross sections evaluated in Refs. [43,44] on the basis of boson-exchange diagrams. For an explicit description of the parametrizations employed we refer the reader to Eqs. (14) and (18) and Tables 1-3 in Ref. [43] for  $\rho, \omega$  and  $\phi$  production in pion-baryon and baryon-baryon channels. The  $\eta$  cross section from  $pp$  collisions is taken in line with the boson exchange calculation in Ref. [44], which can be fitted as

$$\sigma_{pp \rightarrow pp\eta}(\sqrt{s}) = a \frac{\sqrt{s} - \sqrt{s_0}}{b + (\sqrt{s} - \sqrt{s_0})^2} \quad (4)$$

with  $a = 0.4$  mb and  $b = 0.552$  GeV<sup>2</sup> while  $\sqrt{s_0}$  is the  $\eta$  production threshold. This parametrization also reproduces the  $\eta$  production data from the PINOT Collaboration [45] rather well. The  $pn \rightarrow pn\eta$  cross section is taken to be about 6 times the  $pp \rightarrow pp\eta$  cross section close to threshold in line with the new data from the WASA collaboration [46]. The production of  $\eta$  mesons in pion-nucleon collisions as well as  $\eta$  scattering and reabsorption on nucleons is taken from Ref. [47] employing the experimental data from [48] and using detailed balance as well as the known branching ratios of the  $N(1535)$  to pions and  $\eta$ -mesons. The respective  $\eta$  absorption cross section was found in Ref. [49] (Fig. 2) to be well in line with the experimental  $\eta$  photoproduction data on nuclei (see below).

Apart from the production cross sections of the vector mesons  $\rho$  and  $\omega$  their final state interactions with nucleons have to be considered. For the  $\rho$  we adopt the resonance coupling model specified in Section 2 of Ref. [50] whereas for the  $\omega$  we use the total and inelastic cross sections (Eqs. (34), (35)) of Ref. [51] which are less constraint by experimental data. The latter uncertainty, however, plays no essential role in the present analysis because the  $\omega$ -mesons dominantly decay in the vacuum and thus do not contribute to the dilepton invariant mass spectrum below 0.6 GeV.

As noted above, the transport approach (HSD) was found to describe reasonably well hadronic data at SIS energies as well as hadronic and dilepton data at SPS energies [14,23,31,40].

### III. $M_T$ SCALING

In relativistic heavy-ion collisions at BEVALAC/SIS energies the nuclei can be compressed up to about 3 times normal nuclear matter density  $\rho_0$ . In the hot compression zone the nucleons are excited to baryonic resonances which decay by emitting mesons and the produced mesons then can be absorbed, re-emitted and re-scattered.

Information about the degree of equilibration can be obtained from  $m_T$  spectra, where  $m_T = (p_T^2 + m^2)^{1/2}$  and  $p_T$  is the transverse momentum of a particle with mass  $m$ . In this case the spectrum  $1/m_T^2 d\sigma/dm_T$  is of Boltzmann type  $\sim \exp(-\beta m_T)$  with a slope parameter  $\beta$  being related to the global (inverse) temperature at freeze-out in the absence of flow.

The transverse-mass spectra of  $\pi^0$  and  $\eta$  mesons in heavy-ion collisions at SIS energies were recently measured by the TAPS collaboration [36–38] where a  $m_T$  scaling has been observed for both mesons. Such a universal property of the meson spectra at SIS energies has been predicted by the Quark Gluon String Model calculations in Ref. [52] for the Ar + Ca system. In the remainder of this section we will thus systematically investigate  $m_T$  spectra for nucleus-nucleus collisions at SIS energies within the transport approach specified above.

In Fig. 1 we compare the results of our calculation for the transverse-mass spectra of  $\pi^0$  and  $\eta$  mesons with the TAPS data. The upper part shows the  $m_T$  spectra for  $\pi^0$ 's (dashed histogram) and  $\eta$ 's (solid histogram) for C + C at 1.0 A·GeV in the rapidity interval  $0.42 \leq y \leq 0.74$  and at 2.0 A·GeV for  $0.8 \leq y \leq 1.08$ . The experimental data – the open circles and solid squares correspond to  $\pi^0$  and  $\eta$  mesons, respectively – are taken from Ref. [37]. The theoretical results as well as the experimental data at 2.0 A·GeV here are multiplied by a factor of  $10^2$ . The middle part corresponds to Ca + Ca at 1.0 A·GeV for  $0.48 \leq y \leq 0.88$  (multiplied by  $10^{-1}$ ) and at 2.0 A·GeV for  $0.8 \leq y \leq 1.1$  in comparison with the data from Ref. [38]. The lower part shows the calculated  $m_T$  spectra for Ni + Ni at 1.93 A·GeV for  $0.8 \leq y \leq 1.1$  in comparison with the data from Ref. [38].

As seen from Fig. 1, the HSD transport model gives a reasonable description of the  $m_T$  spectra of pions and  $\eta$ 's as measured by the TAPS collaboration without incorporating any

medium modifications for both mesons. It is important to point out that these calculations are parameter-free in the sense that all production cross sections for  $\eta$  mesons are extracted from experimental data in the vacuum and the  $\eta$ -nucleon elastic and inelastic cross sections are obtained by using detailed balance on the basis of an intermediate  $N(1535)$  resonance.

#### IV. IN-MEDIUM $\rho$ PROPAGATOR

The dilepton production is calculated perturbatively by including the contributions from the Dalitz-decays  $\Delta \rightarrow Nl^+l^-$ ,  $N^* \rightarrow Nl^+l^-$ ,  $\pi^0 \rightarrow \gamma l^+l^-$ ,  $\eta \rightarrow \gamma l^+l^-$ ,  $\omega \rightarrow \pi^0 l^+l^-$  and the direct dilepton decays of the vector mesons  $\rho, \omega$  and  $\phi$ , where the  $\rho$  and  $\phi$  meson may be produced in  $\pi^+\pi^-$  and  $K\bar{K}$  or  $\pi\rho$  collisions, respectively. For a detailed description of  $\Delta, N^*$  Dalitz decays we refer the reader to Ref. [33]; the dilepton decays of the  $\eta$  and vector mesons ( $\omega, \phi$ ) are described in Ref. [31].

The dilepton radiation from  $\rho$  mesons is calculated as

$$\frac{dN_{l^+l^-}}{dM} = -Br \frac{2M}{\pi} \text{Im}D_\rho(q_0, q; \rho_B, T), \quad (5)$$

where  $D_\rho$  is the  $\rho$ -meson propagator in the hadronic medium depending on the baryon density  $\rho_B$  and temperature  $T$  as well as on energy  $q_0$  and 3-momentum  $q \equiv |\vec{q}|$  in the local rest frame of the baryon current ('comoving' frame) while  $Br \simeq 4.5 \times 10^{-5}$  is the experimental branching ratio to dileptons. The invariant mass  $M$  is related to the  $\rho$ -meson 4-momentum in the nuclear medium as

$$M^2 = q_0^2 - q^2, \quad (6)$$

while

$$\text{Im}D_\rho = \frac{1}{3}(\text{Im}D_\rho^L + 2\text{Im}D_\rho^T) \quad (7)$$

is spin averaged over the longitudinal and transverse part of the  $\rho$ -propagator,

$$\text{Im}D_\rho^{L,T}(q_0, q; \rho_B, T) = \frac{\text{Im}\Sigma_\rho^{L,T}(q_0, q; \rho_B, T)}{|M^2 - (m_\rho^{(0)})^2 - \Sigma_\rho^{L,T}(q_0, q; \rho_B, T)|^2}. \quad (8)$$



Following Refs. [26,53] the  $\rho$ -meson selfenergy  $\Sigma_\rho^{L,T}(q_0, q, \rho_B, T)$  is obtained by combining the effects of the different hadronic interactions:

$$\Sigma_\rho^{L,T} = \Sigma_{\rho\pi\pi}^{L,T} + \Sigma_{\rho BB^{-1}}^{L,T} + \Sigma_{\rho\pi a_1}^{L,T} + \Sigma_{\rho K K_1}^{L,T}. \quad (9)$$

The explicit evaluation of the various selfenergy components is discussed in detail in Ref. [26].

We here employ an improved version in the following respects:

- (a) in addition to p-wave  $\rho N \rightarrow B$  interactions ( $B=N, \Delta, N(1720)$  and  $\Delta(1905)$ ) we also account for s-wave excitations into  $N(1520)$ ,  $\Delta(1620)$  and  $\Delta(1700)$  resonances (the corresponding coupling constants are, as usual, estimated from the  $\rho N$  partial decay width);
- (b) the coupling of the resonances to (virtual) photons is calculated within the improved vector dominance model of Kroll, Lee and Zumino [54] to avoid overestimates of the  $B \rightarrow N\gamma$  branching ratios. This leads to a modification in the coupling of the transverse part of the  $\rho$  propagator entering Eqs. (5), (11) such that the combination  $(m_\rho^{(0)})^4 \text{Im}D_\rho^T(q_0, q; \rho_B, T)$  is replaced by the 'transition form factor'

$$\begin{aligned} \bar{F}^T(q_0, q; \rho_B) &= -\text{Im}[\Sigma_{\rho\pi\pi}^T + \Sigma_{\rho\pi a_1}^T + \Sigma_{\rho K K_1}^T] |d_\rho - 1|^2 - \text{Im}\Sigma_{\rho BB^{-1}}^T |d_\rho - r_B|^2 \\ d_\rho(q_0, q; \rho_B) &= \frac{M^2 - \Sigma_{\rho\pi\pi}^T - \Sigma_{\rho\pi a_1}^T - \Sigma_{\rho K K_1}^T - r_B \Sigma_{\rho BB^{-1}}^T}{M^2 - (m_\rho^{(0)})^2 - \Sigma_\rho^T}, \end{aligned} \quad (10)$$

where

$$r_B = \frac{\mu_B}{\frac{f_{\rho BN}}{m_\rho} \frac{(m_\rho^{(0)})^2}{g}}$$

denotes the ratio of the photon coupling to its value in the naive VDM.

- (c) the medium modifications of the two-pion selfenergy  $\Sigma_{\rho\pi\pi}$  are extended to arbitrary 3-momentum within the recently developed model of Urban *et al.* [55].

The combined  $\rho$ -meson selfenergy is then further constrained by experimental information on  $\gamma p$  and  $\gamma A$  absorption cross sections as described in Ref. [53]. With the aforementioned

improvements (a) to (c) a satisfactory description of the photoabsorption data, which represent the  $M^2 \rightarrow 0$  limit of the dilepton regime, can be achieved on protons as well as on nuclei. In fact, the melting of the resonance structures (above the  $\Delta$  mass), as seen in the photoabsorption data on nuclei [56], can be explained by the broadening of the higher resonances due to a strong coupling to the short-lived  $\rho$ -meson in the medium [53]. This provides a proper basis to assess the dilepton radiation originating from in-medium  $\pi\pi$  annihilation and  $\rho$  decays in A + A collisions at BEVALAC/SIS energies.

As an example – relevant for the heavy-ion reactions at BEVALAC/SIS energies – we show in Fig. 2 the spin averaged  $-\text{Im}D_\rho(q_0, q; \rho_B, T)$  in the approach of Ref. [26] (including the modifications (a) to (c)) as a function of the invariant mass  $M$  and the 3-momentum  $q$  for a temperature of 70 MeV at  $\rho_B = 0, \rho_0, 2\rho_0$  and  $3\rho_0$ , respectively (note that at this temperature about 10% of the nucleons are excited into  $\Delta$ 's such that  $\rho_N \simeq 0.9\rho_B$ ). With increasing baryon density we find the  $\rho$  spectral function to increase substantially in width showing only minor structures at high density. Thus the lifetime of the  $\rho$ -meson in the nuclear medium becomes very short due to well established hadronic interactions.

Furthermore, we will also employ the  $\rho$  spectral function from Ref. [27] which is calculated by taking only the resonance-holes states (without the correction Eq. (10)) into account including, however, all nucleon resonances up to a mass of  $\approx 1.9$  GeV. In addition, in the latter calculation the feedback of the in-medium  $\rho$  spectral function on the resonance widths is taken into account selfconsistently, i.e. iterated out at given nuclear matter density and 3-momentum. In Fig. 3 we show for comparison the spectral function from Ref. [27] for  $\rho = 0, \rho_0, 2\rho_0$  and  $3\rho_0$  at temperature  $T = 0$ . While the overall structure is similar to that in Fig. 2 the spectral functions in the approach of Ref. [26] are smoother at low invariant mass and the structures at small momenta  $q$ , which result from a selfconsistent treatment of the resonance widths in Ref. [27], are washed out.

The cross section for the pion annihilation channel  $\pi^+\pi^- \rightarrow \rho^0 \rightarrow e^+e^-$  is taken in line with Ref. [57] as

$$\sigma_{\pi^+\pi^-\rightarrow e^+e^-}(M) = -\frac{16\pi^2\alpha^2}{g_{\rho\pi\pi}^2} \frac{1}{k^2M^2} (m_\rho^{(0)})^4 \text{Im}D_\rho(q_0, q; \rho_B, T) \quad (11)$$

where  $k = (M^2 - 4m_\pi^2)^{1/2}/2$  is the pion 3-momentum in the center-of-mass frame and  $\alpha$  is the fine structure constant. The  $\rho\pi\pi$  coupling constant and bare  $\rho$  mass  $m_\rho^{(0)}$  are fixed to reproduce p-wave  $\pi\pi$  scattering and the pion electromagnetic form factor in free space [26,27].

Our dynamical calculations are carried out as follows: the time-evolution of the proton-nucleus or nucleus-nucleus collision is described within the covariant transport approach HSD [40,31] without any dropping vector meson masses. Whenever a  $\rho$ -meson is produced in the course of the hadronic cascade (by baryon-baryon, meson-baryon or pion-pion collisions), its 4-momentum in the local rest frame of the baryon current is recorded together with the information on the local baryon density, the local 'transverse' temperature and its production source. We note that the definition of a local temperature is model dependent; here we have used a logarithmic fit to the transverse  $p_t$  spectra of mesons at midrapidity. Without going into a detailed discussion of this issue we note that our results for dilepton spectra do not change within the numerical accuracy when using a constant temperature  $T = 70$  MeV at BEVALAC energies since  $\text{Im}D_\rho$  depends rather weakly on  $T$  (at fixed nucleon density).

## V. DILEPTON SPECTRA IN COMPARISON TO BEVALAC DATA

In Fig. 4 we present the calculated dilepton invariant mass spectra  $d\sigma/dM$  for Ca + Ca (upper part) and C + C (lower part) at the bombarding energy of 1.0 A·GeV integrated over impact parameter and compare them with the new experimental data of the DLS collaboration [6] including the DLS acceptance filter (version 4.1) as well as a mass resolution  $\Delta M/M = 10\%$ . The thin lines indicate the individual contributions from the different production channels; *i.e.* starting from low  $M$ : Dalitz decay  $\pi^0 \rightarrow \gamma e^+e^-$  (dashed line),  $\eta \rightarrow \gamma e^+e^-$  (dotted line),  $\Delta \rightarrow N e^+e^-$  (dashed line),  $\omega \rightarrow \pi^0 e^+e^-$  (dot-dashed line),  $N^* \rightarrow N e^+e^-$  (dotted line), proton-neutron bremsstrahlung (dot-dashed line),  $\pi N$  bremsstrahlung (dot-dot-dashed line); for  $M \approx 0.8$  GeV:  $\omega \rightarrow e^+e^-$  (dot-dashed line),  $\rho^0 \rightarrow e^+e^-$  (dashed

line),  $\pi^+\pi^- \rightarrow \rho \rightarrow e^+e^-$  (dot-dashed line). The pion annihilation channel as well as the direct decay of the vector mesons here have been calculated with the 'free'  $\rho$  spectral function. The full solid line represents the sum of all sources.

Our present result is consistent with that from Ref. [35] at low invariant mass  $M \leq 0.4$  GeV. However, the contributions from direct decays of  $\rho$  and  $\omega$  mesons are somewhat larger because novel elementary production cross sections for pion-baryon collisions from Ref. [43] were taken into account as well as  $\rho$  and  $\omega$  elastic and inelastic scattering processes with nucleons using the cross sections from Ref. [50,51]. As seen from Fig. 4 the new BEVALAC data cannot be properly described in terms of a 'free'  $\rho$  spectral function. The discrepancy between the data and the calculations for Ca+Ca as well as for C+C at  $0.15 \leq M \leq 0.4$  GeV is about a factor of 3-5. At  $M \sim m_\rho$  the calculation is within the error bars except for the last experimental point.

The description of the DLS data is slightly improved when including the  $\rho$  spectral functions from Ref. [26] (cf. Fig. 2) or Ref. [27] (cf. Fig. 3). In Fig. 5 we show the dilepton spectra (full solid line) for Ca + Ca (upper part) and C + C (lower part) at 1.0 A·GeV calculated with the  $\rho$  spectral function from Ref. [26] (Fig. 2) in comparison with the data [6]. The same comparison is carried out in Fig. 6 for the spectral function (at T=0) from Ref. [27] (Fig. 3). The dashed lines correspond to the channel  $\rho^0 \rightarrow e^+e^-$  while the dot-dashed lines indicate the contribution from  $\pi^+\pi^- \rightarrow \rho \rightarrow e^+e^-$  as described in Section 4. The full  $\rho$  spectral functions lead to a shift of the pion annihilation contribution to the small invariant mass region as well as to a broadening of the  $\rho$ -meson contribution in both approaches. We note that in our transport approach the pions are on-shell, thus we can not probe the  $\rho$ -spectral function in the reactions  $\pi^+\pi^- \rightarrow \rho^0 \rightarrow e^+e^-$  below the two pion threshold at  $M < 2m_\pi$ . The tails from the  $\pi^+\pi^-$  annihilation and  $\rho$  meson at  $M < 2m_\pi$ , which are seen in Figs. 5 and 6, exist only due to the finite mass resolution of  $\Delta M/M \simeq 10\%$ . We note that we discard meson-baryon ( $mB$ ) and meson-meson ( $mm$ ) bremsstrahlung channels as well as the Dalitz decays of the baryon resonances (stemming from secondary pion induced reactions) in order to avoid double counting when employing the full  $\rho$  spectral functions.

Due to the on-shell treatment of pions in the transport approach the dilepton spectra for  $M \simeq 2m_\pi$  might not be properly described. In order to investigate the effects from an off-shell propagation of pions in the channel  $\pi^+\pi^- \rightarrow \rho^0 \rightarrow l^+l^-$ , we have performed additional calculations within the thermodynamical approach used in Ref. [26] at SPS energies. For BEVALAC energies we use exactly the same procedure, however, with temperature and density profiles obtained from the HSD transport model [40] for Ca + Ca at 1.0 A·GeV. The solid curves in Fig. 7 correspond to the sum of all channels and the  $\rho$  decay (from  $\pi^+\pi^-$  annihilation and direct production), respectively, while the dashed lines are from the transport model (cf. Fig. 5). As seen from Fig. 7 an off-shell pion propagation leads to a large enhancement in the  $\rho$ -decay channel especially below the  $2\pi$  threshold. However, considering all channels simultaneously, the maximum increase – compared to the transport model – is only 30%. Thus, all independent calculations give practically the same results; the new DLS data are underestimated at least by a factor of 3 for  $0.15 \leq M \leq 0.4$  GeV even when taking into account the modification of the  $\rho$  meson properties in the nuclear medium.

## VI. DROPPING $\eta$ MASS?

According to the general scaling idea of Brown and Rho [58]  $\eta$  mesons might also change their properties in the medium. In this section we examine the possibility of a dropping  $\eta$  mass at BEVALAC/SIS energies as well as for  $\eta$  photoproduction on nuclei. For our analysis we use a linear extrapolation of the  $\eta$  mass,

$$m_\eta^* = m_\eta^0 \left( 1 - \alpha \frac{\rho_B}{\rho_0} \right), \quad (12)$$

with a 'large' value for  $\alpha \approx 0.18$ , which might be considered as an upper limit. According to Eq. (12) the  $\eta$  mass decreases at normal nuclear matter density by 18%. The maximum baryon density reached in central Ca + Ca collisions is about  $2.5\rho_0$ , thus the dropping  $\eta$  mass leads to an essential reduction of the  $\eta$  production threshold in  $BB$  and  $mB$  collisions and to a strong enhancement of the  $\eta$  population in heavy-ion collisions. Similar, but less pronounced effects are expected for the  $\eta$  photoproduction on nuclei for densities  $\rho_B \leq \rho_0$ .

### A. Nucleus-nucleus collisions

In Fig. 8 we show the dilepton spectra (full solid line) for Ca + Ca (upper part) and C + C (lower part) at 1.0 A·GeV calculated with the full  $\rho$  spectral function [26] and a dropping  $\eta$  mass in comparison with the data from Ref. [6]. As seen from Fig. 8, the dropping  $\eta$  mass scenario together with the full spectral function approach leads to a good reproduction of the BEVALAC data.

However, the dropping  $\eta$  mass scenario does not yield the observed  $m_T$  scaling. The transverse-mass spectra of  $\pi^0$  and  $\eta$  mesons for C + C in  $0.42 \leq y \leq 0.74$  (lower part) and Ca + Ca for  $0.48 \leq y \leq 0.88$  (upper part) at 1.0 A·GeV are shown in Fig. 9. The assignment of lines is the same as in Fig. 1. The dot-dashed histograms correspond to the  $\eta$   $m_T$ -spectra obtained within the dropping  $\eta$  mass scenario. The  $m_T$  scaling in this case is violated by about a factor of 3 especially at low  $m_T \simeq m_\eta$ .

Thus we find that the simple  $\eta$  dropping mass scheme is not consistent with the  $m_T$  scaling observed by the TAPS collaboration. A more sophisticated scenario for the  $\eta$  self-energy (like momentum dependent  $\eta$  potentials etc. [59]) still has to be studied.

### B. $\eta$ photoproduction on nuclei

Since the dynamics of nucleus-nucleus collisions at SIS energies is rather complex it is useful to have further constraints on the  $\eta$  properties in the medium as e.g. tested in  $\eta$  photoproduction on nuclei where the kinematical conditions are much better under control. The latter problem has been addressed in detail in Refs. [60,61] on the basis of transport approaches, where further details of the explicit calculations can be found. Since in the present study we want to explore the possible consequences of a dropping  $\eta$  mass at finite nuclear density we reparameterize the  $\eta$  photoproduction on a proton as

$$\sigma_{\gamma p \rightarrow \eta p}(\sqrt{s}) = a(1-x)^b \exp\left(-(\sqrt{s} - \sqrt{s_0})^2/c\right) \quad (13)$$

with  $x = \sqrt{s_0}/\sqrt{s}$ ,  $a = 161.5 \mu b$ ,  $b = 0.571$  and  $c = 8.9 \cdot 10^{-3} \text{ GeV}^2$ , which provides a good description of the experimental data from Refs. [62,63]. The  $\eta$  photoproduction on a neutron is found experimentally to be 2/3 as that on a proton; we adopt the same ratio for our calculations. The parametrization (13) as a function of the invariant energy above threshold  $\sqrt{s} - \sqrt{s_0}$  now allows to simulate  $\eta$  photoproduction with a dropping  $\eta$  mass according to Eq. (12). We note, that the parametrization (13) assumes the photoproduction to be dominated by phase space or the invariant energy above threshold; this assumption still has to be controlled by microscopic in-medium calculations on  $\eta$  photoproduction and here only serves as an estimate.

The results of our transport calculations for  $\eta$  production on  $^{40}\text{Ca}$  for photon energies from 600 - 780 MeV are displayed in Fig. 10 in comparison to the data from Ref. [49]. The full line corresponds to the bare  $\eta$  mass whereas the dashed line is obtained for a dropping mass according to Eq. (12) with  $\alpha = 0.18$ . The excitation function clearly indicates that the  $\eta$  properties do not change much in the medium except for a strong  $\eta$  absorption which is about 65 % in case of  $^{40}\text{Ca}$  (cf. Ref. [61]); the dropping  $\eta$ -mass scenario leads to enhanced  $\eta$  cross sections especially at low photon energy which are not observed experimentally. Thus also  $\eta$  photoproduction data exclude a dramatic change of the  $\eta$  properties in the medium as possibly 'requested' by the DLS data (cf. Fig. 4).

## VII. ANISOTROPY OF THE $\eta$ ANGULAR DISTRIBUTION

As proposed by the DLS collaboration [6] the inconsistency between the DLS and TAPS data might be due to differences in the experimental acceptance – mid-rapidity for TAPS versus forward rapidity for DLS – and a strong anisotropy of the  $\eta$  angular distribution. The TAPS group calculated the total  $\eta$  cross section from a model where mesons are emitted isotropically from a thermal source at  $y_{cm}$ . Using the mid-rapidity TAPS data and a simple thermodynamical model the DLS collaboration reproduces the result from our previous calculation [35].

In Fig. 11 we, therefore, present the result of our transport calculation for the angular distribution of  $\eta$  mesons for Ca + Ca at 1.0 A·GeV. Mainly due to rescattering in matter the  $\eta$  angular distribution is anisotropic; however, this anisotropy is not very pronounced. As was estimated by the TAPS collaboration, the implementation of this anisotropy gives at maximum a 20% correction for the total  $\eta$  cross section [64]. Thus, the anisotropy effect according to our transport calculations cannot explain an enhancement by a factor of 3-7 in the new DLS dilepton data.

### VIII. SUMMARY

On the basis of the covariant transport approach HSD [40] we have studied dilepton production and  $m_T$  scaling in C + C and Ca + Ca collisions at BEVALAC energies. We have found that the  $m_T$  scaling of  $\pi^0$  and  $\eta$  observed by the TAPS collaboration is reproduced by the transport calculation even for the small system C + C when incorporating no medium effects for the pions and etas.

Various contributions are taken into account for dilepton production: the Dalitz-decays of  $\Delta$ ,  $N^*$  resonances and  $\pi^0$ ,  $\eta$ ,  $\omega$  mesons, proton-neutron bremsstrahlung,  $\pi N$  bremsstrahlung as well as the direct dilepton decays of the vector mesons  $\rho$  and  $\omega$ . It was shown that the new DLS data [6] are underestimated by a factor of 6-7 in the transport calculations for invariant mass  $0.15 \leq M \leq 0.4$  GeV when no medium effects are involved as in our previous calculations [35].

Including the  $\rho$  meson modifications in the medium (according to the spectral functions from Refs. [26,27]) slightly improves the agreement with the data, but the discrepancy is still about a factor of 3. This also holds for the thermodynamical approach [26] where an off-shell propagation of pions is taken into account. A simple dropping  $\eta$  mass scheme together with the full  $\rho$  spectral function can lead to dilepton spectra that are in a good agreement with the DLS data. However, the  $m_T$ -scaling of  $\pi^0$ 's and  $\eta$ 's observed by the TAPS collaboration cannot be reproduced within this dropping  $\eta$  mass scenario anymore.



The dropping mass scenario also is clearly incompatible with the  $\eta$  photoproduction data on nuclei. Also the anisotropy of the  $\eta$  angular distribution due to rescattering effects in matter - as obtained from our transport calculation - is much too small to explain the enhancement of the dilepton yield at  $0.15 \leq M \leq 0.4$  GeV as observed by the DLS collaboration.

### ACKNOWLEDGMENTS

The authors are grateful for many helpful discussions with M. Appenheimer, R. Averbeck, G.E. Brown, R. Holzmann, C. M. Ko, H. Lenske, V. Metag, A. Sibirtsev, V.D. Toneev, P. Vogt and Th. Weidmann. They especially like to thank U. Mosel for valuable suggestions and a careful reading of the manuscript. Furthermore, they are indebted to M. Urban for providing the results on the finite 3-momentum dependence in the two-pion selfenergy and to M. Post and W. Peters for the  $\rho$  spectral function from Ref. [27] prior to publication. One of us (RR) acknowledges support from the Alexander-von-Humboldt foundation as a Feodor-Lynen fellow. This work was supported in part by the U.S. department of energy under contract No. DE-FG02-88ER40388 and a grant from the National Science Foundation, NSF PHY 94-21309.

## REFERENCES

- [1] G. Brown and M. Rho, Phys. Rev. Lett. 66 (1991) 2720.
- [2] M. C. Birse, J. Phys. G20 (1994) 1537.
- [3] G. Roche et al., Phys. Rev. Lett. 61 (1988) 1069.
- [4] C. Naudet et al., Phys. Rev. Lett. 62 (1989) 2652.
- [5] G. Roche et al., Phys. Lett. B226 (1989) 228.
- [6] R.J. Porter et al., Phys. Rev. Lett. 79 (1997) 1229.
- [7] G. Agakichiev et al., Phys. Rev. Lett. 75 (1995) 1272.
- [8] Th. Ullrich et al., Nucl. Phys. A610 (1996) 317c; A. Drees, Nucl. Phys. A610 (1996) 536c.
- [9] M. A. Mazzoni, Nucl. Phys. A566 (1994) 95c; M. Masera, Nucl. Phys. A590 (1995) 93c.
- [10] T. Åkesson et al., Z. Phys. C68 (1995) 47.
- [11] C. Baglin et al., NA38, Phys. Lett. B220 (1989) 471; B251 (1990) 465.
- [12] M. Gonin et al., Nucl. Phys. A610 (1996) 404c.
- [13] G. Q. Li, C. M. Ko, and G. E. Brown, Phys. Rev. Lett. 75 (1995) 4007.
- [14] W. Cassing, W. Ehehalt, and C. M. Ko, Phys. Lett. B363 (1995) 35.
- [15] V. Koch and C. Song, Phys. Rev. C54 (1996) 1903.
- [16] D. K. Srivastava, B. Sinha, and C. Gale, Phys. Rev. C53 (1996) R567.
- [17] L. A. Winckelmann, C. Ernst, L. Gerland, J. Konopka, S. Soff et al., nucl-th/9610042.
- [18] M. Herrmann, B. Friman, and W. Nörenberg, Nucl. Phys. A560 (1993) 411.
- [19] M. Asakawa, C. M. Ko, P. Lévai, and X. J. Qiu, Phys. Rev. C46 (1992) R1159.

- [20] G. Chanfray and P. Schuck, Nucl. Phys. A545 (1992) 271c.
- [21] R. Rapp, G. Chanfray, and J. Wambach, Phys. Rev. Lett. 76 (1996) 368.
- [22] C. M. Ko, G. Q. Li, G. E. Brown, and H. Sorge, Nucl. Phys. A610 (1996) 342c.
- [23] W. Cassing, W. Ehehalt, and I. Kralik, Phys. Lett. B377 (1996) 5.
- [24] T. Hatsuda and S. Lee, Phys. Rev. C46 (1992) R34.
- [25] B. Friman and H. J. Pirner, Nucl. Phys. A617 (1997) 496.
- [26] R. Rapp, G. Chanfray and J. Wambach, Nucl. Phys. A617 (1997) 472.
- [27] W. Peters, M. Post, H. Lenske, S. Leupold, and U. Mosel, nucl-th/9708004, Nucl. Phys. A, in press.
- [28] F. Klingl, N. Kaiser, and W. Weise, Nucl. Phys. A 624 (1997) 527.
- [29] S. Leupold, W. Peters and U. Mosel, nucl-th/9708016.
- [30] W. Cassing, E. L. Bratkovskaya, R. Rapp, and J. Wambach, nucl-th/9708020, Phys. Rev. C, in press.
- [31] E. L. Bratkovskaya and W. Cassing, Nucl. Phys. A619 (1997) 413.
- [32] L. Xiong, Z. G. Wu, C. M. Ko, and J. Q. Wu, Nucl. Phys. A512 (1990) 772.
- [33] Gy. Wolf, G. Batko, W. Cassing, U. Mosel, K. Niita, and M. Schäfer, Nucl. Phys. A517 (1990) 615; Gy. Wolf, W. Cassing and U. Mosel, Nucl. Phys. A552 (1993) 549.
- [34] K.K. Gudima, A.I. Titov and V.D. Toneev, Sov. Jour. of Nucl. Phys. 55 (1992) 1715.
- [35] E. L. Bratkovskaya, W. Cassing and U. Mosel, Phys. Lett. B 376 (1996) 12.
- [36] O. Schwalb et al., Phys. Lett. B 321 (1994) 20; F. D. Berg et al., Phys. Rev. Lett. 72 (1994) 977.
- [37] R. Auerbeck et al., Z. Phys. A359 (1997) 65.

- [38] M. Appenheimer et al., GSI Annual Report 1996, p.58.
- [39] S. Teis, Ph.D. Thesis, University of Giessen, 1997, unpublished.
- [40] W. Ehehalt and W. Cassing, Nucl. Phys. A602 (1996) 449.
- [41] K. Weber, B. Blättel, W. Cassing, H.-C. Dönges, V. Koch, A. Lang, and U. Mosel, Nucl. Phys. A 539 (1992) 713.
- [42] W. Cassing, Z. Phys. A 327 (1987) 447.
- [43] A. Sibirtsev, W. Cassing and U. Mosel, Z. Phys. A 358 (1997) 357.
- [44] T. Vetter, A. Engel, T. Biro and U. Mosel, Phys. Lett. B 263 (1991) 153.
- [45] E. Chiavassa et al., Phys. Lett. B 322 (1994) 270.
- [46] H. Calén et al., Phys. Rev. Lett., in press.
- [47] W. Cassing, G. Batko, T. Vetter, and G. Wolf, Z. Phys. A 340 (1991) 51.
- [48] Landolt-Börnstein, New Series, vol. I/12, ed. H. Schopper, Springer, Berlin (1988).
- [49] M. Röbig-Landau et al., Phys. Lett. B 373 (1996) 45.
- [50] A. Sibirtsev and W. Cassing, nucl-th/9712009, Nucl. Phys. A, in press.
- [51] Ye. S. Golubeva, L. A. Kondratyuk and W. Cassing, Nucl. Phys. A 625 (1997) 832.
- [52] K. K. Gudima, M. Ploszajczak, V.D. Toneev, Phys. Lett. B 328 (1994) 249.
- [53] R. Rapp, M. Urban, M. Buballa and J. Wambach, preprint SUNY-NTG-97-48 and nucl-th/9709008, Phys. Lett. B., in press.
- [54] N. M. Kroll, T. D. Lee and B. Zumino, Phys. Rev. 157 (1967) 1376.
- [55] M. Urban, M. Buballa, R. Rapp and J. Wambach, to be published.
- [56] N. Bianchi et al., Phys. Lett. B 299 (1993) 219; B 309 (1993) 5; B 325 (1994) 333.

- [57] P. Koch, Z. Phys. C 57 (1993) 283.
- [58] G. E. Brown and M. Rho, Phys. Rev. Lett. 66 (1991) 2720.
- [59] H.C. Chiang, E. Oset and L.C. Liu, Phys. Rev. C 44 (1991) 738.
- [60] A. Hombach et al., Z. Physik A 352 (1995) 223.
- [61] M. Effenberger, A. Hombach, S. Teis, and U. Mosel, Nucl. Phys. A 614 (1997) 501.
- [62] B. Krusche et al., Phys. Rev. Lett. 74 (1995) 3736.
- [63] B. Schoch, Prog. Part. Nucl. Phys. 34 (1995) 43.
- [64] R. Holzman, Proceedings of the International Workshop on Soft Dilepton Production, Berkeley, Aug. 20-22, 1997; [http://csa4.lbl.gov/dilepton\\_workshop/proceedings.html](http://csa4.lbl.gov/dilepton_workshop/proceedings.html).

## FIGURES

FIG. 1. The calculated transverse-mass spectra of  $\pi^0$  and  $\eta$  mesons in comparison with the TAPS data. The upper part shows the  $m_T$  spectra for  $\pi^0$ 's (dashed histogram) and  $\eta$ 's (solid histogram) for C + C at 1.0 A·GeV in the rapidity interval  $0.42 \leq y \leq 0.74$  and at 2.0 A·GeV for  $0.8 \leq y \leq 1.08$ . The experimental data – open circles and solid squares correspond to  $\pi^0$  and  $\eta$  mesons, respectively – are taken from Ref. [37]. The theoretical results as well as the experimental data at 2.0 A·GeV are multiplied by a factor of  $10^2$ . The middle part corresponds to Ca + Ca at 1.0 A·GeV for  $0.48 \leq y \leq 0.88$  (multiplied by  $10^{-1}$ ) and at 2.0 A·GeV for  $0.8 \leq y \leq 1.1$  in comparison with the data from Ref. [38]. The lower part shows the calculated  $m_T$  spectra for Ni + Ni at 1.93 A·GeV at rapidities  $0.8 \leq y \leq 1.1$  in comparison with the data from Ref. [38].

FIG. 2. The (negative) imaginary part of the  $\rho$  propagator averaged over the longitudinal and transverse components (where the latter contain the correction Eq. (10)) as a function of the invariant mass  $M$  and the momentum  $q$  for baryon densities of 0,  $1 \rho_0$ ,  $2 \rho_0$ , and  $3 \rho_0$  and temperature  $T = 70$  MeV in the extended approach of Ref. [26]. Note the different absolute scales in the individual figures.

FIG. 3. The (negative) imaginary part of the  $\rho$  propagator averaged over the longitudinal and transverse components as a function of the invariant mass  $M$  and the momentum  $q$  for baryon densities of 0,  $1 \rho_0$ ,  $2 \rho_0$ , and  $3 \rho_0$  at temperature  $T = 0$  MeV in the approach of Ref. [27]. Note the different absolute scales in the individual figures.

FIG. 4. The dilepton spectra (full solid line) for Ca + Ca (upper part) and C + C (lower part) at 1.0 A·GeV calculated with the 'free'  $\rho$  spectral function including the DLS acceptance filter (version 4.1) as well a mass resolution  $\Delta M/M = 10\%$  in comparison with the data from Ref. [6]. The thin lines indicate the individual contributions from the different production channels including the DLS acceptance and mass resolution; *i.e.* starting from low  $M$ : Dalitz decay  $\pi^0 \rightarrow \gamma e^+ e^-$  (dashed line),  $\eta \rightarrow \gamma e^+ e^-$  (dotted line),  $\Delta \rightarrow N e^+ e^-$  (dashed line),  $\omega \rightarrow \pi^0 e^+ e^-$  (dot-dashed line),  $N^* \rightarrow N e^+ e^-$  (dotted line), proton-neutron bremsstrahlung (dot-dashed line),  $\pi N$  bremsstrahlung (dot-dot-dashed line); for  $M \approx 0.8$  GeV:  $\omega \rightarrow e^+ e^-$  (dot-dashed line),  $\rho^0 \rightarrow e^+ e^-$  (dashed line),  $\pi^+ \pi^- \rightarrow \rho \rightarrow e^+ e^-$  (dot-dashed line).

FIG. 5. The dilepton spectra (full solid line) for Ca + Ca (upper part) and C + C (lower part) at 1.0 A·GeV calculated with the full  $\rho$  spectral function in the extended approach of Ref. [26] in comparison with the data from Ref. [6]. The assignment of the individual contributions is the same as in Fig. 4.

FIG. 6. The dilepton spectra (full solid line) for Ca + Ca (upper part) and C + C (lower part) at 1.0 A·GeV calculated with the full  $\rho$  spectral function in the extended approach of Ref. [27] in comparison with the data from Ref. [6]. The assignment of the individual contributions is the same as in Fig. 4.

FIG. 7. The dilepton spectra for Ca + Ca at 1.0 A·GeV calculated within the thermodynamical approach [26] (solid lines) and within the transport model (dashed lines).

FIG. 8. The dilepton spectra (full solid line) for Ca + Ca (upper part) and C + C (lower part) at 1.0 A·GeV calculated with the full  $\rho$  spectral function in the extended approach of Ref. [26] for the dropping  $\eta$  mass scenario in comparison with the data from Ref. [6]. The assignment of the individual contributions is the same as in Fig. 4.

FIG. 9. The transverse-mass spectra of  $\pi^0$  and  $\eta$  mesons for Ca + Ca in the rapidity interval  $0.48 \leq y \leq 0.88$  (upper part) and C + C for  $0.42 \leq y \leq 0.74$  (lower part) at 1.0 A·GeV. The assignment is the same as in Fig. 1. The dot-dashed histograms correspond to the  $\eta$   $m_T$ -spectra obtained within the dropping  $\eta$  mass scenario.

FIG. 10. The calculated  $\eta$  photoproduction cross section on  $^{40}\text{Ca}$  as a function of the photon energy  $E_\gamma$  in comparison to the data from [49]. The solid histogram displays our results for a bare  $\eta$  mass whereas the dashed histogram corresponds to the dropping  $\eta$  mass scenario (12).

FIG. 11. The calculated angular distribution of  $\eta$  mesons for Ca + Ca at 1.0 A·GeV in the center-of-mass system.



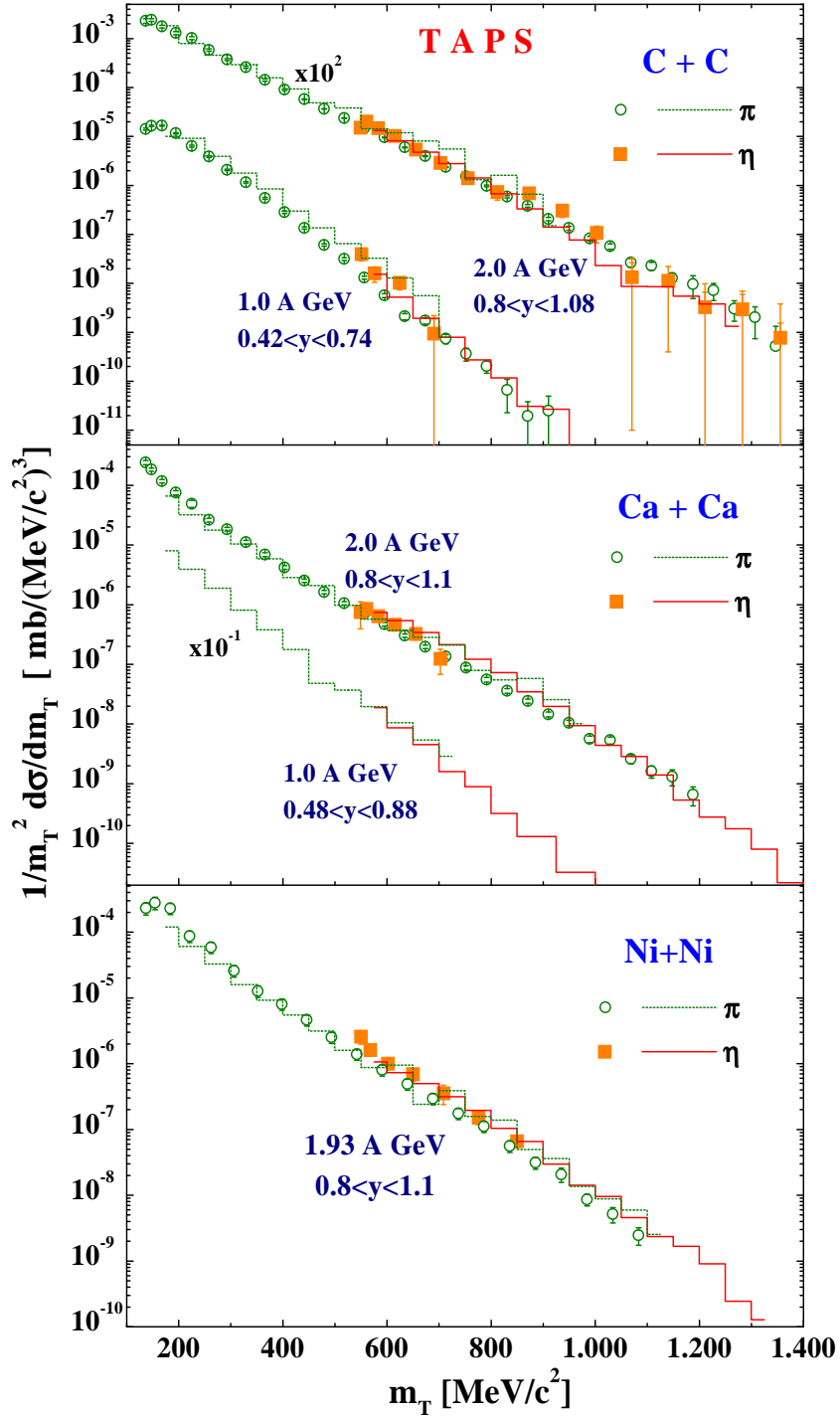


Fig. 1

$-\text{Im } D_\rho(M, q, \rho_B, T)$  [ $\text{GeV}^{-2}$ ]  
 $T=70 \text{ MeV}$

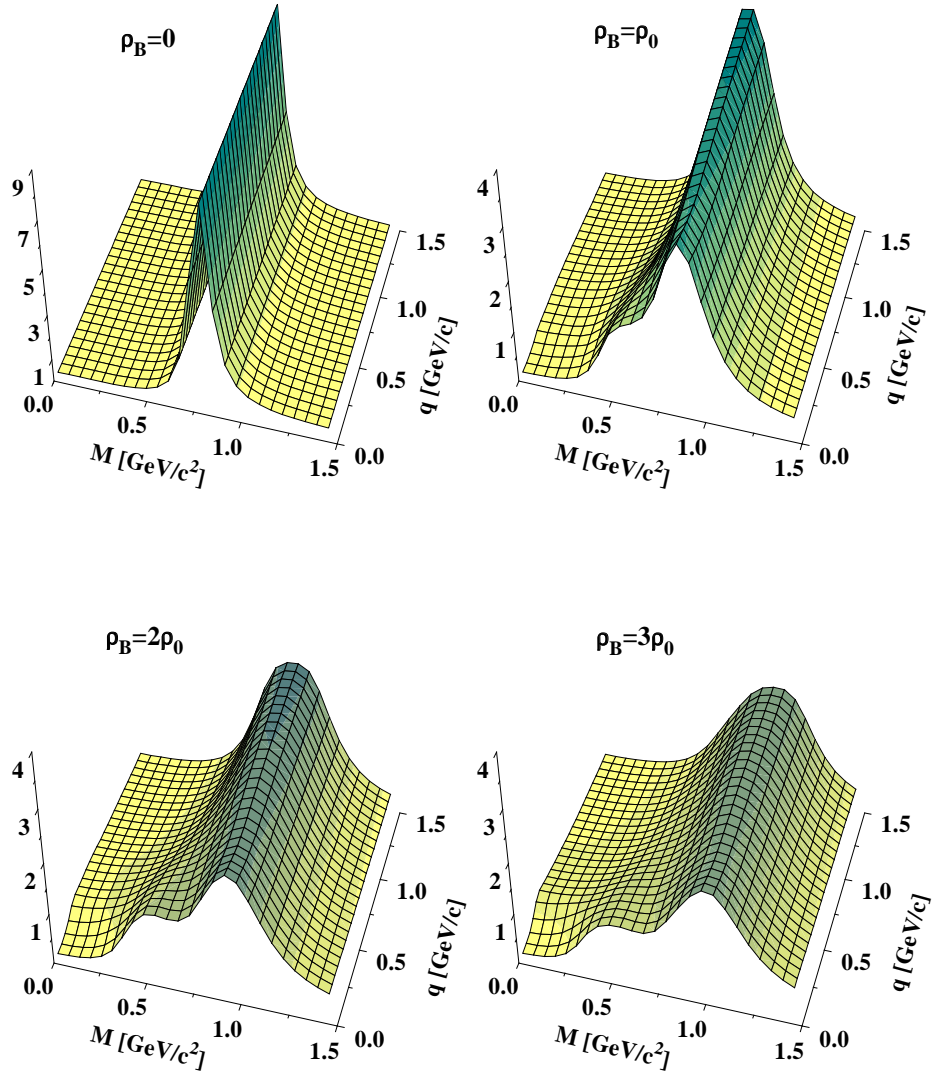


Fig. 2

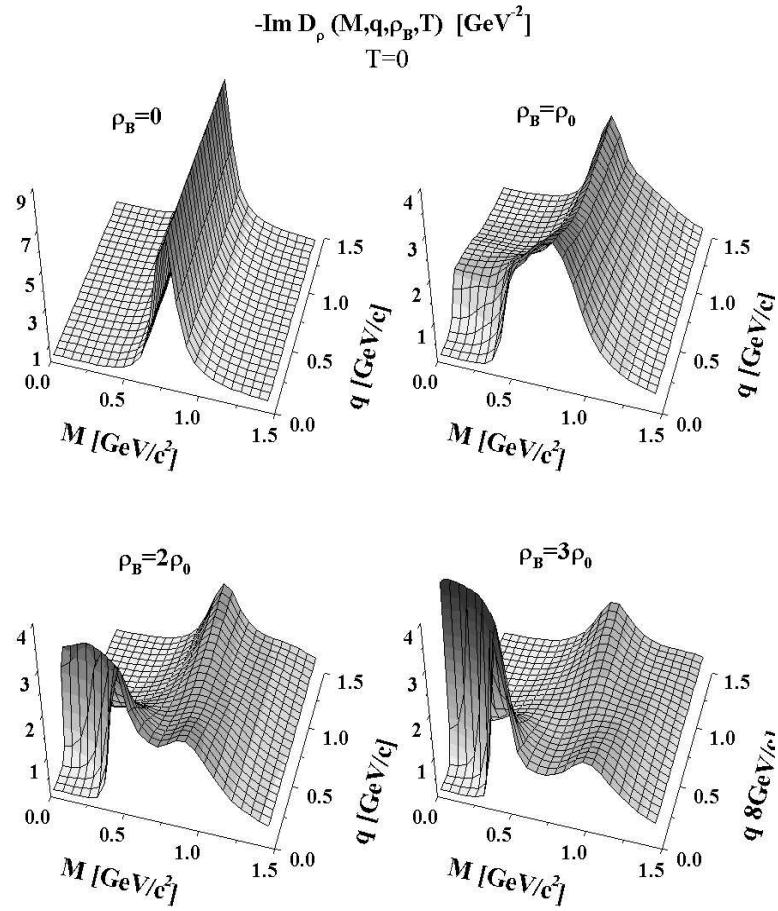


Fig. 3

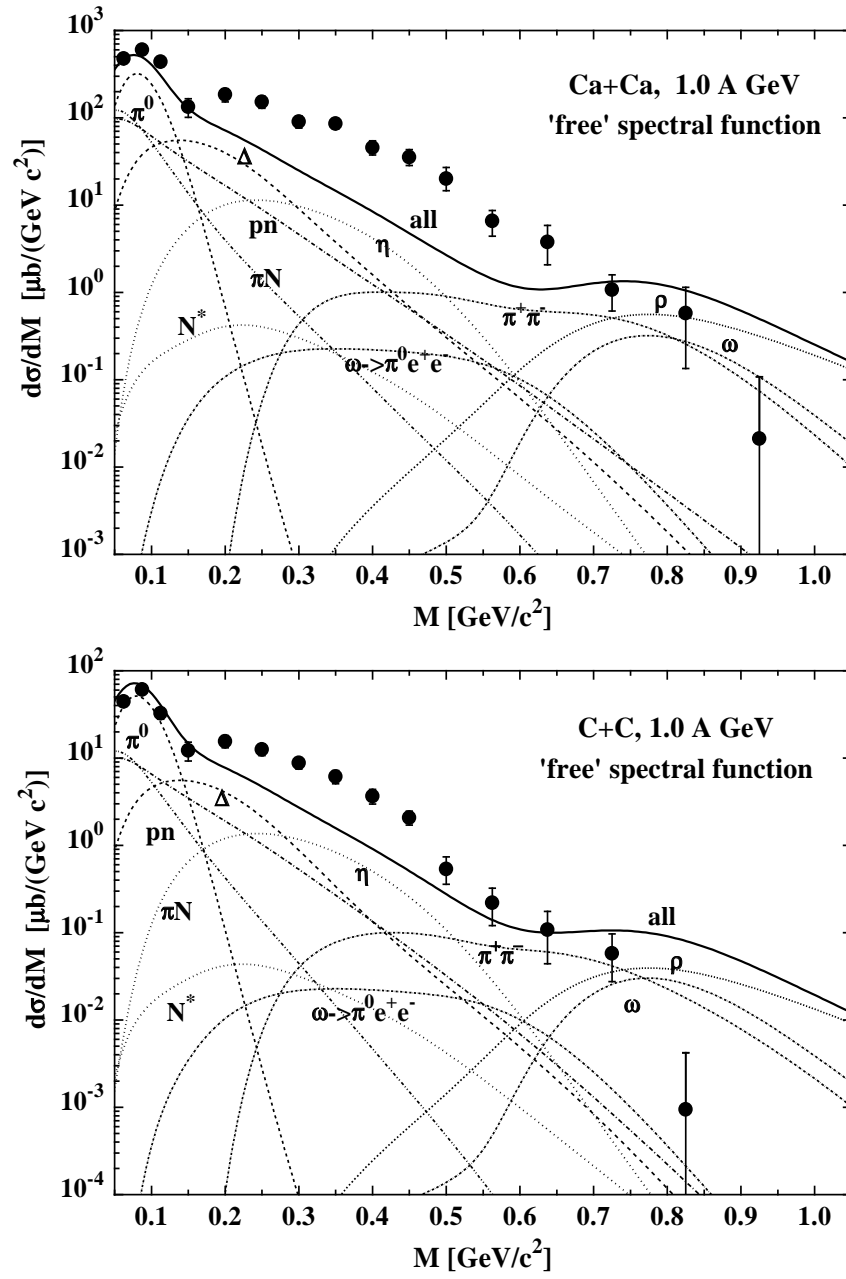


Fig. 4

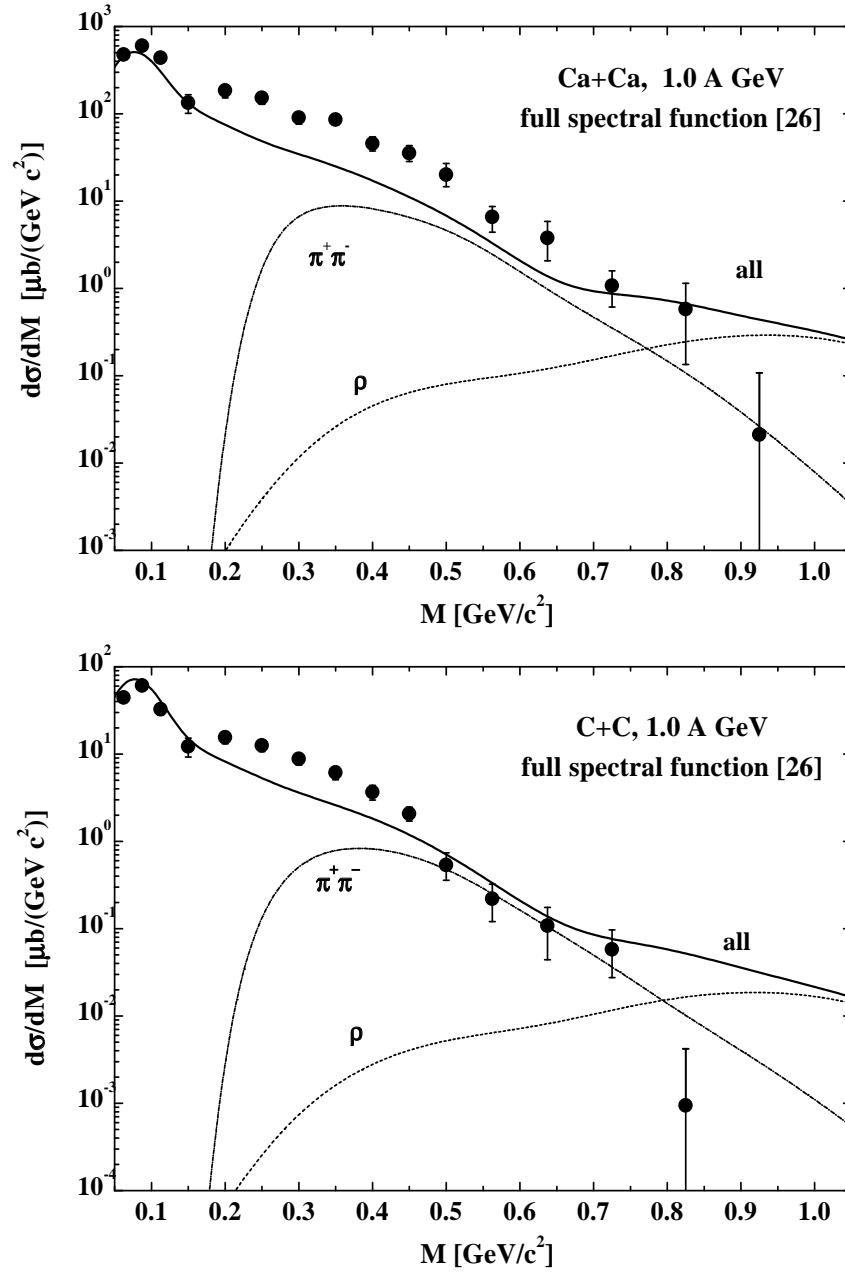


Fig. 5

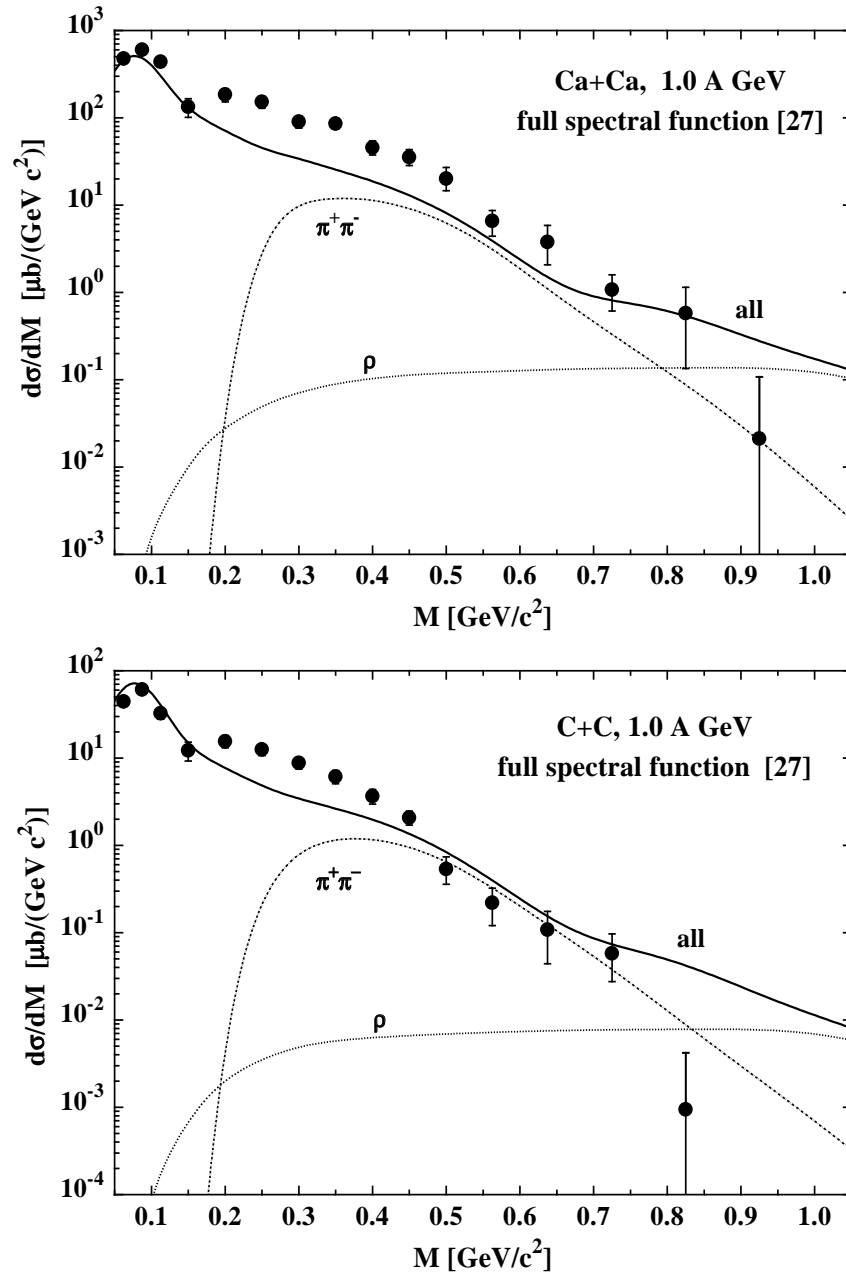


Fig. 6

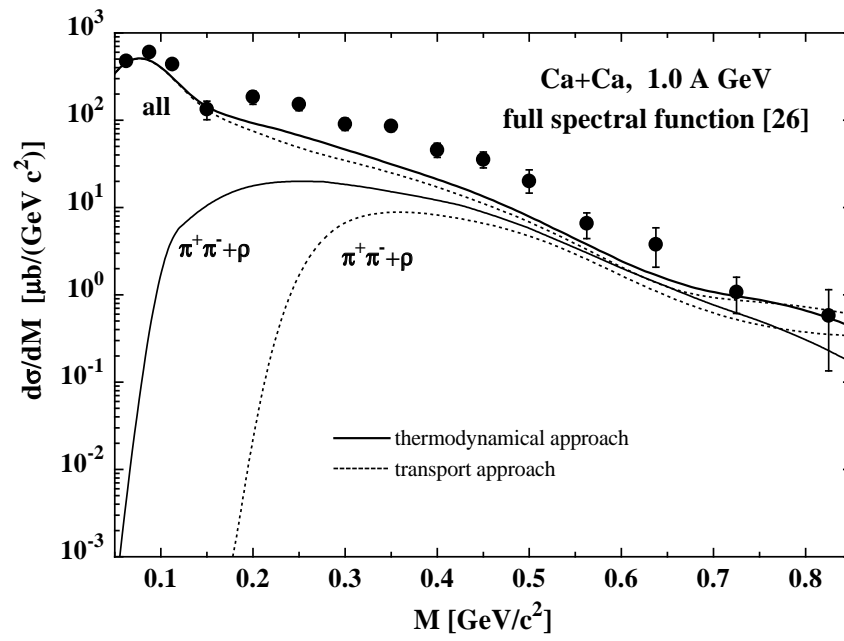


Fig. 7

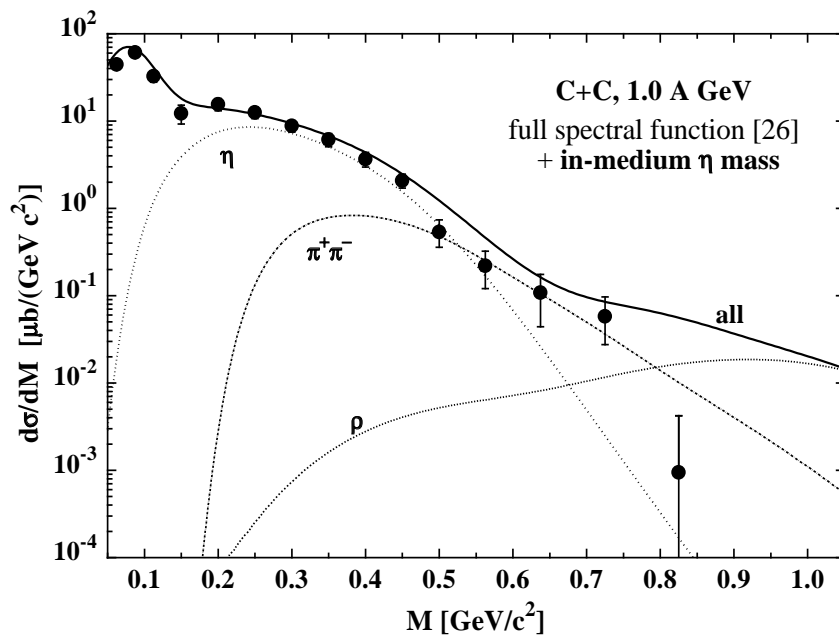
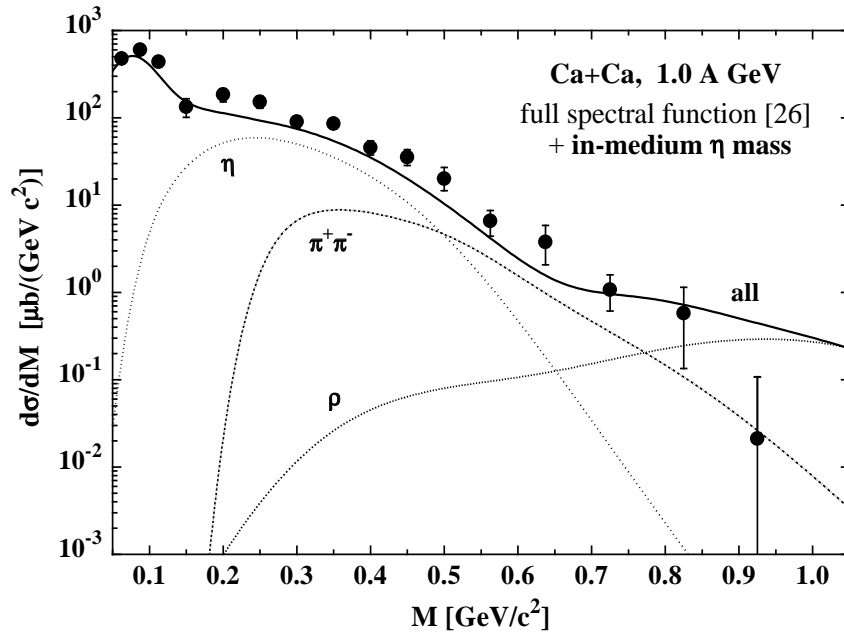


Fig. 8



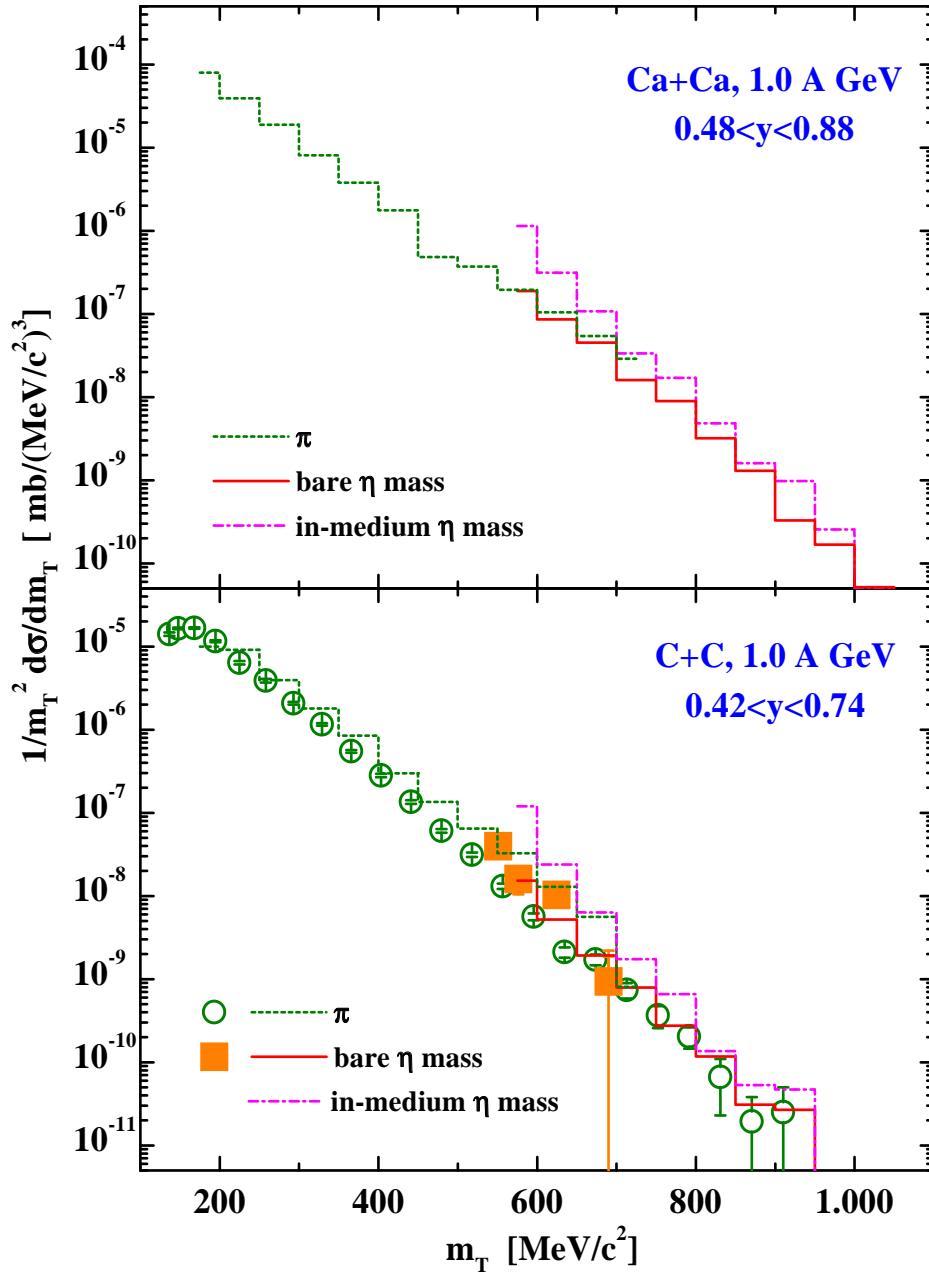


Fig. 9

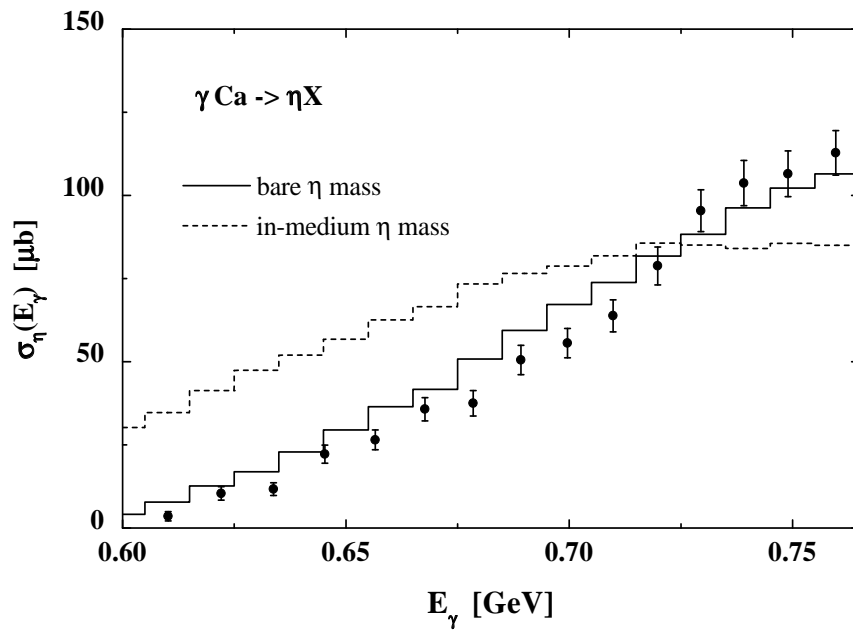


Fig. 10

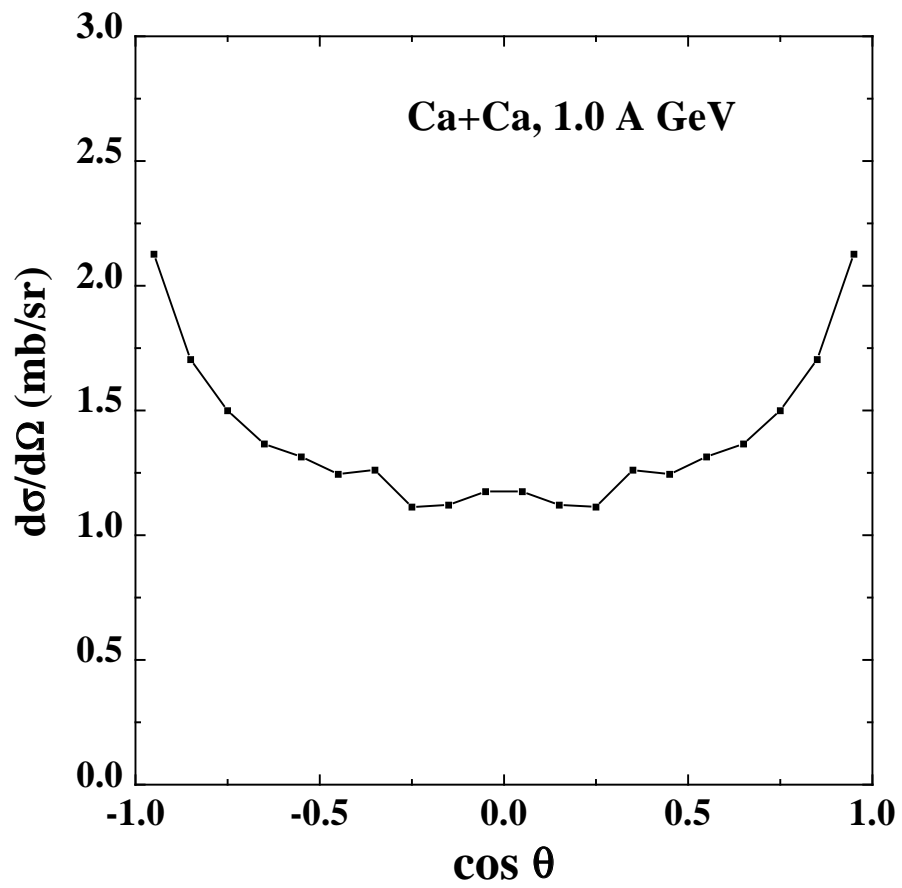


Fig. 11